# Some Aspects on the Welding Characteristics and Formation of Microstructures in a Newly Developed Coated Electrode for Austempered Ductile Iron (ADI)

**Tapan Sarkar, Ajit Kumar Pramanick and Tapan Kumar Pal***

Welding Technology Centre, Metallurgical and Material Engg. Dept., Jadavpur University, Kolkata-700032
*Corresponding Author Email: tkpal.ju@gmail.com

**ABSTRACT**

In this study, six different coated electrodes were manufactured to select compatible one for ADI and only two electrodes were further studied (Trial 3 and Trial 4)to check their compatibility. Welding conditions were established to obtain crack free weld deposit on DI plate by varying preheat (200°C, 300°C and 400°C for 1hour) as well as PWHT (maintaining same preheat temperature) at constant heat input using two selected electrodes. Only preheating at 300°C was possible to obtain sound weld for Trial 3, whereasboth preheat (300°C) and PWHT (300°C) were required for Trial 4. Although the as-deposited microstructures of FZ and PMZ consisting of ledeburitic carbide and alloyed pearlite in both the electrodes were same, the amount of microstructural constituents varied significantly. More ledeburitic carbide and less alloyed pearlite were observed in Trial 3 compared to Trial 4. However, microstructures of HAZ for both the electrodes showed bainitic and pearlite. Austempering heat treatment comprising of austenitization at 900°C for 2 hr and austempering at two different temperatures (300°C and 350°C) for different holding time was carried out for both the weld deposits. Interestingly, for both the weld deposits austempered microstructures show bainitic ferrite and retained austenite with graphite nodules. Increasing austempering temperature from 300°C and 350°C the lower bainite transformed to upper bainite and vol. % of retained austenite was also increased.

**Keywords:** Electrode development; microstructure; austempering; microhardness

## 1.0 INTRODUCTION

Austempered ductile iron (ADI), a relatively a new material, was invented in the 1950s but was commercialised and successfully achieved in 1970 by the Finish company Kymmene Metall Kyki [1]. The development of ADI is a major achievement in cast iron technology.

ADI is obtained from good quality ductile or nodular cast iron by austempering heat treatment which occurs in two steps e.g. austenitizing and austempering. Austenitizing is done in the temperature range between 871–982°C for sufficient time to obtain complete austenitic matrix followed by quenching the casting to an intermediate temperature range of 260–400°C for 1-4 hr holding and then air cooling [2].

During the austempering process a two stage phase transformation reaction takes place. During first stage the austenite ($\gamma$) transformed to ferrite ($\alpha$) and high carbon enriched austenite ($\gamma$HC).

$$\gamma \rightarrow \alpha + \gamma HC$$

If the austempering time is too long a second stage reaction starts and high carbon enriched austenite further decomposes into ferrite and ε-carbide.

$$\gamma H \rightarrow \alpha + \varepsilon\text{-carbide}$$

Since the ε-carbide is a detrimental phase constituent (make the material brittle), this stage II reaction must be avoided during austempering process.

The microstructure of ADI thus consists of ferrite and high carbon austenite and is often refereed as "ausferrite" rather than bainite. Because of these microstructure, ADI has emerged an important engineering materials with properties

similar to cast and wrought steel. The advantages of ADI include high ultimate tensile strength (850-1400 MPa), reasonable ductility (4-10%), higher fatigue resistance [3], and good wear resistance [4-6]. Additionally, ADI is also 10% less dense than steel, giving higher specific strength. Because of these advantages, ADI is increasingly being used in many commercial engineering applications, including automotive components (transmission gear, gear box, connecting rods, crankshaft) [7], defence (cannon shells, aircraft landing gears), earth moving machinery and railroads etc. [8-11].

However, in all these applications ADI is being used as cast product and thus has restricted its applicability within a certain domain. In order to exploit its potential as an engineering material for several applications, it is necessary to join them. Welding of cast iron is difficult because of high carbon and the presence of graphite. During welding high carbon and graphite are mainly responsible to develop brittle microstructure and defects due to rapid weld thermal cycle. In addition to fusion zone (FZ) and heat affected zone (HAZ), partially transformation zone (PMZ) is also formed in the cast iron weldment. **Fig. 1** shows different zones in cast iron weldment and corresponding temperature in Fe-C phase diagram.

High carbon martensite and carbide cause cast iron material hard, brittle and formation of crack in the joint as well as difficulty in machining [12-15]. However, weldability of cast iron depends on the several factors including [16–23]: (i) type of the cast iron, (ii) chemical composition of the cast iron, (iii) chemical composition of filler metal, (iv) original matrix structure and (v) welding process and preheat/post heat treatment.

Most of the welding performed in cast iron is repair welding. It is either the repair of discontinuities produced during the casting process or those developed in the cast component itself while in service [24]. However, in case of ADI having excellent mechanical properties similar to steel, it could be repaired welding during manufacturing DI or joining DI for converting ADI for structural applications as well. Regarding welding of conventional ductile iron, substantial work was performed to find out suitable welding conditions by varying filler material, preheat temperature and heat input [24-29]. Filler metals like ENi-Cl and ENiFe-Cl overcomed the problems of carbon-pick-up from pearlitic ductile iron and deposited either Ni or Ni-iron weld with the high carbon content and provided necessary strength and ductility. Preheat temperature reduced residual stress and deformation to prevent the cold cracking and reduced hardness in the HAZ. However, the level of 300°C preheat temperature [30] was reported to be optimum temperature, to minimize the effect of carbon pick up from base material along with slow cooling. Heat input also played an important role in the formation and morphology of carbide in the FZ and microstructure formed in the HAZ. A lower heat input, as expected, minimized the width of HAZ relative to FZ, while higher heat input widened the HAZ and FZ.

Commercially available coated electrodes for welding conventional ductile iron include pure nickel (90-97%) [24], stainless steel and iron nickel [31] which are first of all not suitable for converting ADI from DI weld due to poor austemperability and also not cost effective [32]. However, alloying elements such as Cu, Ni, and Mo have been reported to have favourable effect on austemperability. Although coating composition is extremely complex, judicial selection and transfer of such alloying elements through coating in the coated electrode could satisfy the weld metal microstructure requirement imposed by ADI. Furthermore, primarily the flux coating of an SMAW consumable electrode has to fulfil different functions such as arc stability, protect the molten metal from the atmosphere, and refine the weld pool [33-34]. Additionally, the flux coating should be formulated with ingredients that produce a low-density slag, provide proper viscosity for a smoother weld contour and bead shape, out-ofposition welding, promote slag detachability, and reduce spatter and fume.

Unfortunately, the information available on the consumable for welding DI which will respond to isothermal heat treatment and converting ADI is still limited [24, 31]. The challenge of welding ADI therefore lies in developing welding electrodes which will compatible with ductile iron (DI) as well as respond austempering heat treatment in order to produce weld metal having microstructure similar to ADI and also to find out suitable welding conditions for crack free weld.

Successful welding of DI, which will be converted to ADI by austempering heat treatment, therefore requires under-standing of interaction between the composition/ micro-structure of DI; filler metal composition and weld thermal cycle. This paper addresses the development of coated electrode for DI followed by suitable welding procedure to produce crack free welding and finally austempering heat treatment was performed to check the response of heat treatment applied to weld metal. Theoptical microscope (OM), scanning electron microscope (SEM), X-ray diffraction (XRD) and microhardness study were performed to characterize microstructures of the weldments (both as - welded and heat treated conditions).

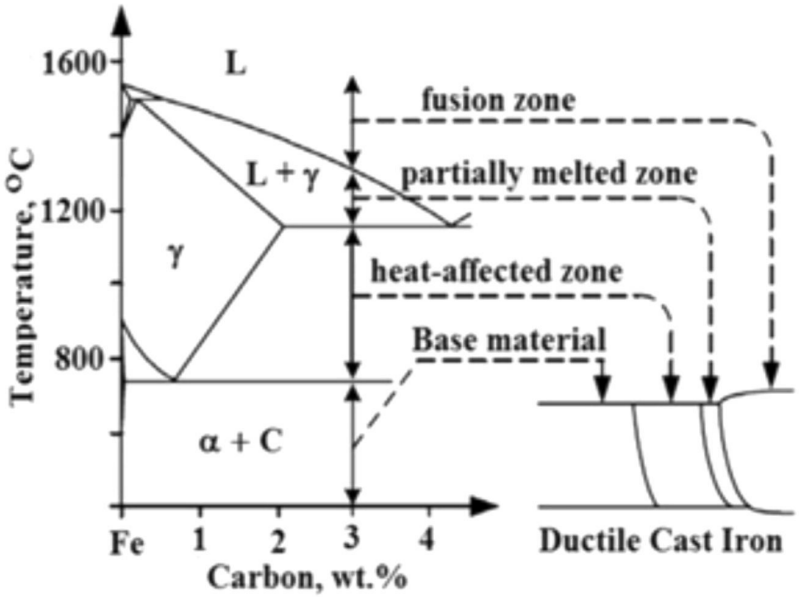


**Fig.1 :** Different zones in cast iron weldment and corresponding temperature in Fe-C phase diagram [35].

## 2.0 EXPERIMENTAL PROCEDURE

### 2.1 Electrode Formulation

The composition of the flux ingredient was varied systematically by changing the different alloying elements, graphite and silicon powders, de-oxidiser etc. in mainly CaO-$SiO_2$-$Al_2O_3$ flux system for developing coated electrode. Typical flux ingredients used in the experiment is given in **Table 1**. Graphite powder was used to add C in weldmetal and Fe-Si was added to stabilize the function of graphite and also to prevent the formation of carbide in weld metal. However, Fe-Al and Fe-Ti were also added as strong deoxidiser to react with oxygen. The addition of Fe-Mo, Fe-Mn and Ni powder were performed to increase the austemperability and hardenability of weld metal. Silicate (14% Na silicate + 4% K silicate) was used as a binder.

### 2.2 Manufacture of Coated Electrode

To produce coated electrode in laboratory extrusion m/c (**Fig. 2**), a 2.5 kg dry powder of flux ingredients was mixed with the help of mixture grinder and liquid binding agent (14% Na silicate + 4% K silicate) was added to make it wet. The cylinder ram in extruder (capacity 280kg/ $cm^2$) compressed the wet flux at a pressure between 90 kg/$cm^2$ to 120 kg/$cm^2$ on extruded die which was fixed at an angle of 30° to the wire centre line. The procedure of electrode extrusion is shown through the flow diagram (**Fig. 3**).

The successful extrusion of the electrode depends on the different factors such as adequate flux coating ratio with good particle size, right amount of binder and slipping agent, proper selection of the core wire diameter, eccentricity of coating etc. Coating thickness depending on the core wire diameter is another important factor of manufacturing electrode

**Table 1 :** Flux composition of developed electrode

| Flux Ingredient | Weight % |
|---|---|
| $BaCo_3$ Powder | 1.2 |
| Acidic Fluorspar Powder | 7 |
| Graphite Powder | 24.5±1 |
| Fe-Si Powder | 18±1 |
| Fe-Ti Powder | 1.5 |
| Ni Powder | 0.85 |
| $BiCo_3$ Powder | 0.2 |
| Fe-Mo Powder | 2.7 |
| Al Powder | 7 |
| Cu Powder | 6 |
| Calcite Powder | 23 |
| Fe powder | 5 |
| $MgCo_3$ Powder | 0.35 |
| Na Alginate Powder | 1.2 |
| CMC Powder | 1.5 |

extrusion. The coating ratio which is the ratio between the electrode diameter and core wire diameter was fixed in the present study as 1.5 and measured by dial indicator.

After extrusion the electrodes were first dried in open air for 24 hours and they were transferred to baking furnace where it was heated at different temperatures for different holding time as shown in **Fig. 4**.

### 2.3 Chemical Pad

Chemical pad was prepared for chemical analysis of weld deposits without dilution. For the present study, chemical pad was prepared by depositing six different types of coated electrodes marked as Trial 1 to Trial 6 on DI base plate. Eight layers of beads (**Fig. 5**) were deposited using current (150A), voltage (24V) and welding speed of 1.7 mm/sec. After completion of the chemical pad, surface of the weld deposits was ground to smooth for spectroscopy analysis.

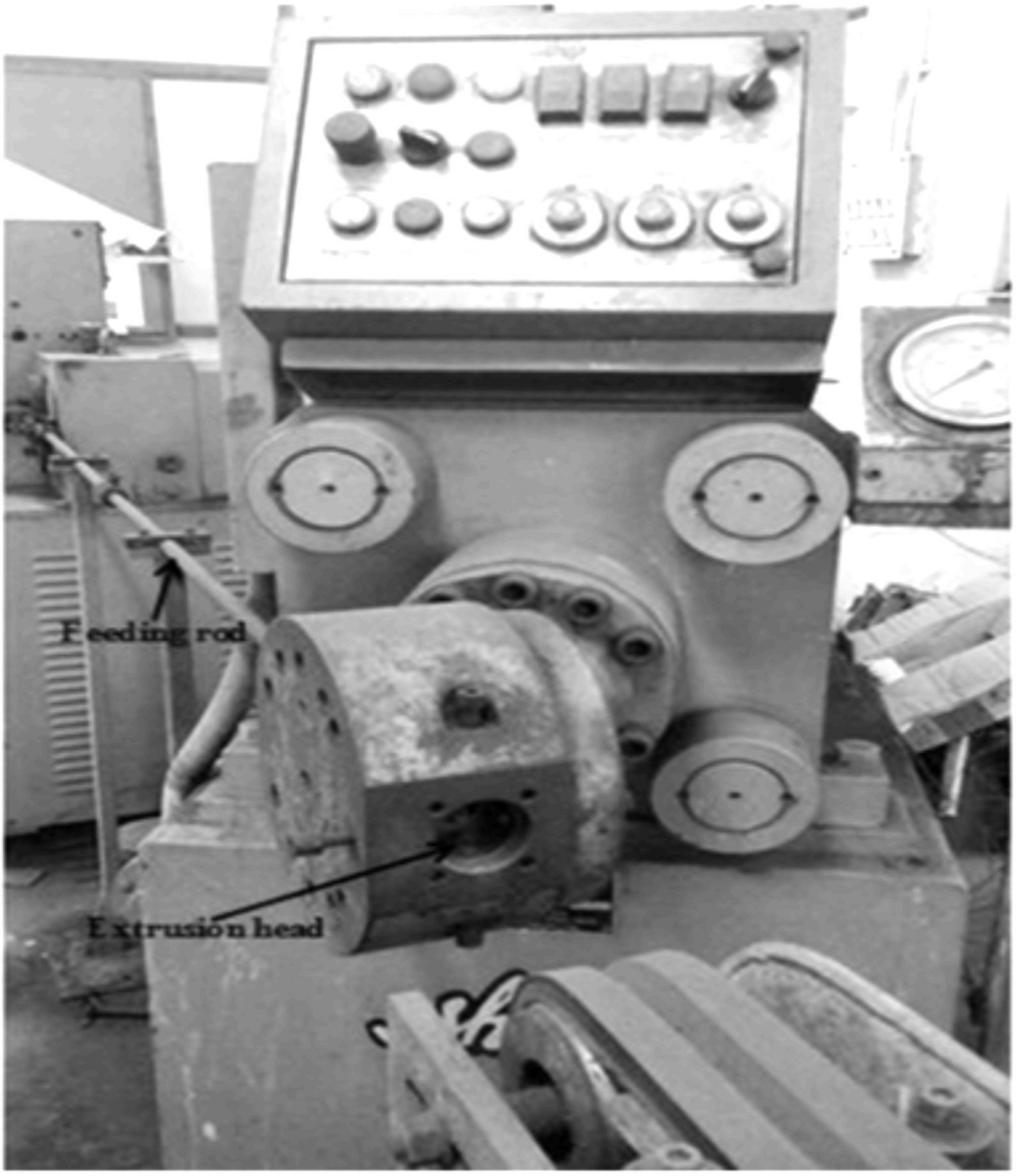


**Fig.2 :** Extrusion Machine used for the work

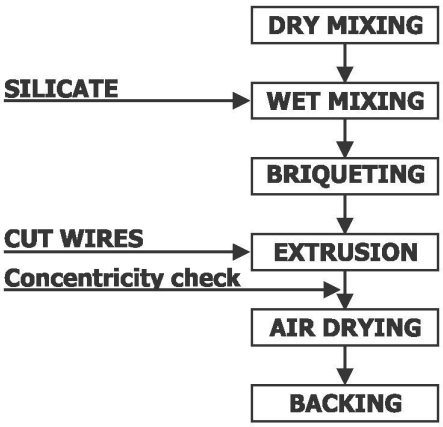


**Fig.3** : Flow diagram of complete extrusion of electrode

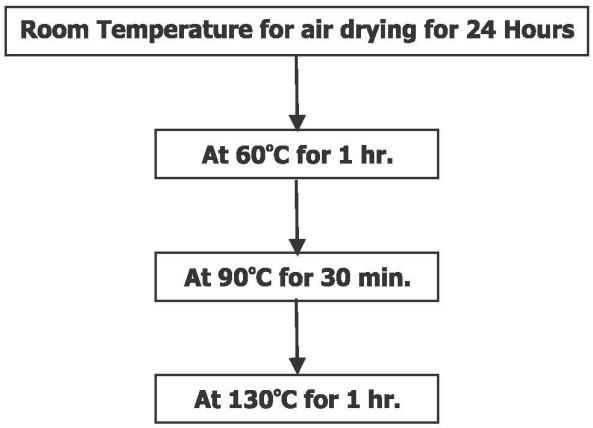


**Fig. 4** : Baking temperature and holding time of extruded electrode

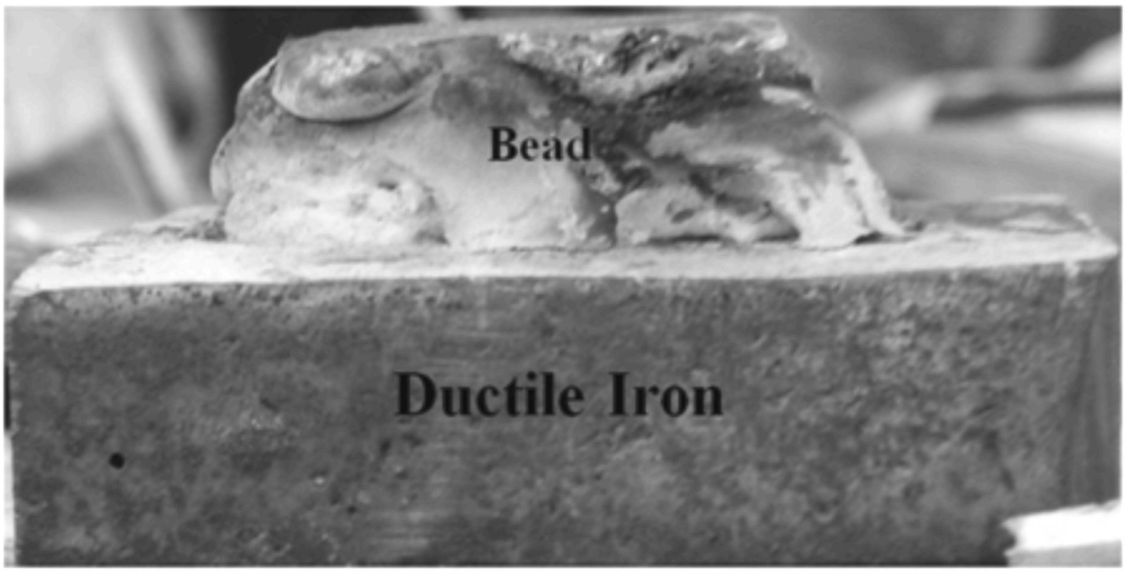


**Fig.5 :** Typical chemical pad formed using developed electrode

### 2.4 Base Material

The material used for this investigation was cast ductile iron of size 220 x 125 x 20 mm, collected from AB casting, Nagpur. The chemical composition of the base material was given in **Table 2.**

### 2.5 Bead-on-plate Study

A single pass bead-on-plate was deposited on DI base plate using each developed coated electrode in flat position under fixed current (150A), voltage (24V) and welding speed of 1.7 mm/sec conditions. Different preheat temperatures as well as with and without post weld heat treatment (PWHT) were used to find out welding conditions (given in **Table 3**) in order to produce crack free weld for two developed electrodes (Trial 3 and Trial 4) which are close to the target composition. Preheat at 200°C, 300°C and 400°C for 1 hour was applied and same preheat temperatures were used as PWHT.

**Table 2 :** Chemical composition of the as cast base material (DI)

| Element (Wt. %) | C | Si | Mn | Mg | Cu | Ni | Mo | Al | Ca | Ba | Bi | S | P | Ti |
|---|---|---|---|---|---|---|---|---|---|---|---|---|---|---|
| Base Material | 2.64 | 2.18 | 0.29 | 0.05 | 0.70 | 0.69 | 0.002 | 0.01 | 0.02 | 0.001 | 0.01 | 0.01 | 0.03 | 0.01 |

**Table 3**: Welding parameters used for bead-on-plate study using two electrodes (Trial-3 and Trial-4)

| Welding Conditions | Applied Voltage (V) | Applied Current (A) | Preheat Temp.°C (1h) | PWHT Temp.°C (1h) | Remarks |
|---|---|---|---|---|---|
| Trial 3 | 24 | 150 | 200 | 200 | Crack |
| | | | 300 | – | No Crack |
| Trial 4 | | | 200 | 200 | Crack |
| | | | 300 | – | Crack |
| | | | 300 | 300 | No Crack |
| | | | 400 | – | Crack |

### 2.6 Heat Treatment

The weld samples of size 15x8x5 mm were cut from bead-on-plate deposits for heat treatment. The isothermalheat treatment process was done in two steps; first the samples were austenitized at 900°C in baking furnace for 2 hr holding time. After that the samples were immediately transferred to saltbath fixed at 300°C and 350°C for 1.5, 2 and 2.5 hr holding time for austempering and finally samples were taken out from the salt bath at respective time interval to allow air cooling upto room temperature. The heat treatment cycle is given in **Fig. 6**.

### 2.7 Metallography and XRD Analysis

The weld samples of size 15x8x5 mm were cut from bead-on-plate deposits for the as-welded microstructural study. Both as-welded and heat treated samples were ground and polished as per standard technique and finally etched with 5% nital solution. The etched samples were examined under optical microscope and photomicrographs were taken at different magnifications (100X, 200X and 500X). For better clarity, samples were also studied under SEM.

X-ray diffraction (XRD) analysis was performed using Cu – Kα radiation with 24 kV and tube current of 40 mA for evaluating the vol. % retained austenite following the procedure of Rundman and Klug[36].

### 2.8 Micro Hardness

Vickers micro hardness test was performed across the weldment at room temperature using 100gf load for 10s holding time.

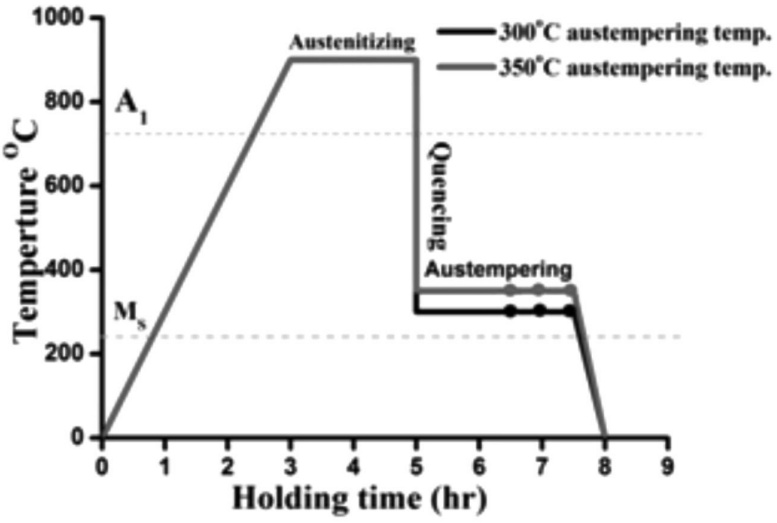


**Fig. 6:** Austempering heat treatment cycle for different temperature and holding time.

**Table 4 :** Chemical composition of the alloying elements (wt. %) in Trial electrodes

| Element wt.% | C | Mn | Si | S | P | Ni | Mo | Cu | Al | Bi | Mg | Ca | Ti |
|---|---|---|---|---|---|---|---|---|---|---|---|---|---|
| Trial 1 | 2.61 | 0.41 | 2.79 | 0.007 | 0.13 | 0.12 | 0.05 | 1.32 | 0.29 | 0.03 | 0.002 | 0.5 | 0.05 |
| Trial 2 | 1.80 | 0.44 | 3.34 | 0.003 | 0.009 | 0.85 | 0.42 | 0.37 | 0.64 | 0.002 | 0.001 | 0.008 | 0.18 |
| Trial 3 | 3.1 | 0.43 | 2.45 | 0.005 | 0.017 | 0.61 | 0.26 | 0.25 | 0.49 | 0.02 | 0.005 | 0.008 | 0.005 |
| Trial 4 | 3.08 | 0.40 | 2.60 | 0.006 | 0.039 | 0.50 | 0.19 | 0.24 | 0.62 | 0.03 | 0.004 | 0.015 | 0.09 |
| Trial 5 | 1.77 | 0.44 | 3.40 | 0.004 | 0.007 | 0.61 | 0.27 | 0.30 | 0.44 | 0.025 | 0.018 | 0.007 | 0.13 |
| Trial 6 | 1.99 | 0.44 | 3.65 | 0.008 | 0.017 | 0.66 | 0.19 | 0.17 | 0.30 | 0.004 | 0.0005 | 0.004 | 0.24 |

## 3.0 RESULTS AND DISCUSSION

### 3.1 Chemical composition of weld metal and slag recovery

The final weld metal chemical composition is usually determined by the slag-metal reactions that take place in the weld pool. Slag-metal reactions are generally studied with a single flux system. Due to complexity of the welding conditions and the non-ideal behaviour of the reactions, it is difficult to make accurate predictions on the effect of specific changes in slag system. Even small changes in the coating composition may result in large variations in the metallurgical processes occurring in the weld pool.

Alloy additions have been made to the weld metal mostly in the forms of metal powders (e.g. Ni, Cu and Al) and ferro-alloys (e.g. Fe-Si, Fe-Mo, Fe-Ti etc.). However, the weld metal chemical content could be adjusted based on the behaviour of specific flux ingredients. An important consideration in the addition of ferro-alloys in fluxes is the recovery of elements. Although some expected recovery of elements from electrode coating was suggested by G. E. Linnert [37], the results of weld metal alloy contents from the expected recovery varied widely. For example, the recovery of Si from Fe-Si in the present investigation is 25% although as per G. E. Linnert recovery of Si is 45%.This could be due to different flux system used leading to competitive reactions occurred in the weld pool.

### 3.2 Bead-on-plate Study

During bead-on-plate study welding conditions mainly preheat temperature and PWHT were varied to obtain sound weld. For Trial 3 electrode crack free welds was obtained at 300°C preheat for 1hr and without PWHT. However, for Trial 4 electrode both preheat at 300°C for 1hr and PWHT maintaining same temperature and time immediate after welding were required to obtain crack free welds. Additional PWHT requirement in case of Trial 4 electrode is probably due to lower Ni ad higher Al content in the weld deposits. The welding conditions to produce crack free welds for Trial 3 and Trial 4 electrodes are given in **Table 5**. Typical bead-on-plate on DI plate with crack and without crack is shown in **Fig. 7**.

**Table 5 :** Typical welding conditions for sound weld in bead-on-plate study

| Welding Conditions | Trial-3 electrode | Trial-4 electrode |
|---|---|---|
| Applied Voltage (V) | 24 | 24 |
| Applied Current (A) | 150 | 150 |
| Preheat Temp.(°C) | 300 (1h) | 300(1h) |
| PWHT Temp.(°C) | 300 (1h) | - |
| Welding speed (mm/sec) | 1.7 | 1.7 |

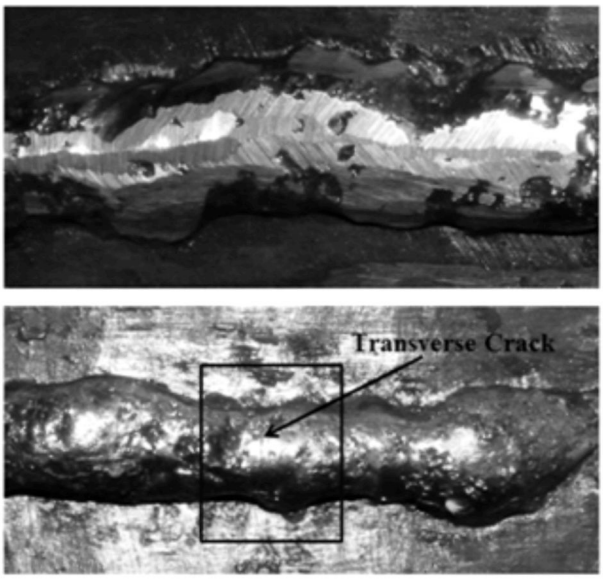


**Fig. 7 :** Deposited bead-on-plate (a) without crack and (b) With Crack (showing transverse crack)

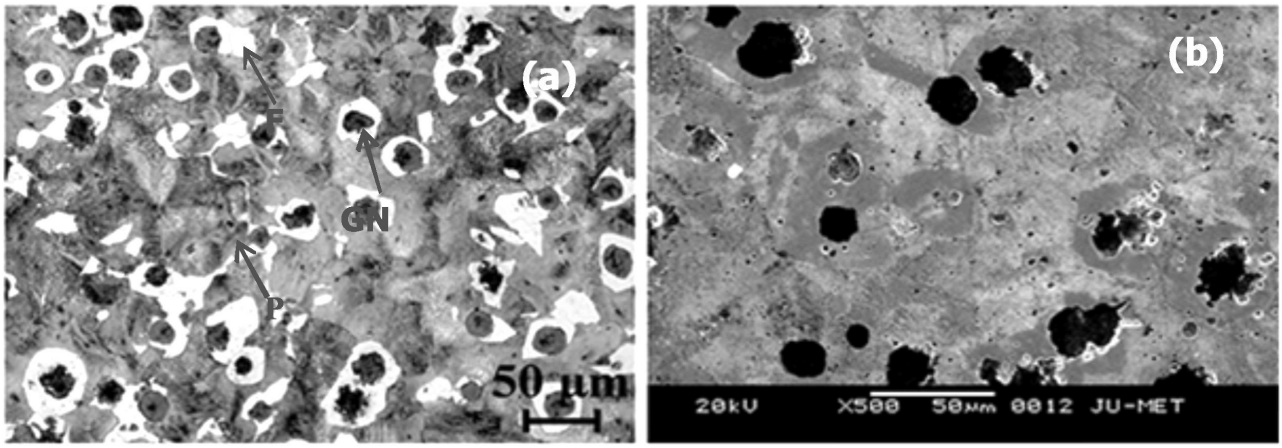


**Fig.8 :** Microstructure of as-cast ductile iron (a) Optical Microstructure, (b) SEM microstructure.

### 3.3 Microstructure of Base Material

The microstructure of the as-cast DI plate as shown in **Fig. 8** consists of graphite nodules in ferrite- pearlite matrix. Though as-cast microstructure shows similar to conventional DI, but it differs in chemical composition. The alloying elements such as Cu, Ni, and Mo have been added (**Table 2**) in order to respond austempering heat treatment.

### 3.4 Microstructure of as-welded bead-on-plate

**Fig. 9 (a-b)** and **Fig. 10 (a-b)** show the microstructures of fusion zone (FZ), Partial melted zone (PMZ) and HAZ for Trial 3 and Trial 4 electrodes respectively. It is observed from **Fig. 9(a)** and **Fig. 10 (a)** that both the FZ microstructures consist of ledeburitic carbide with surrounded by alloyed pearlite and graphite nodules. However, in case of Trial 3 ledeburitic carbide shows continuous in nature, whereas Trail 4 shows dis-continuous carbide. Furthermore, less amount of ledeburitic carbide and more alloyed pearlite are observed in FZ of Trial 4 compared to Trial 3. This is due to the effect of PWHT, which retarded the cooling rate and provided more time for diffusion and presence of higher amount of Si and Al (**Table 4**), which inhibited carbide separation from ledeburitic and thus facilitated to provide more amount of austenite. This austenite ultimately transformed to pearlite at eutectoid temperature.

**Fig. 9 (b)** and **Fig. 10 (b)** show microstructures of PMZ and HAZ. PMZ forms next to the FZ as a boundary to HAZ. Structures formed in PMZ zone are similar to FZ e.g. eutectic ledeburitic carbide and alloyed pearlite with graphite nodules. However, eutectic carbides are coarser and graphite nodules are larger. In PMZ, the portion of the matrix of the base metal near the primary graphite nodules melted during welding, while the remainder of the matrix transformed to austenite. Both the liquid and austenite were enriched with carbon by partial solution of graphite. On cooling the liquid solidified as eutectic carbides, while the high carbon austenite transformed to pearlite. It is to be noted that liquid pool will solidify locally

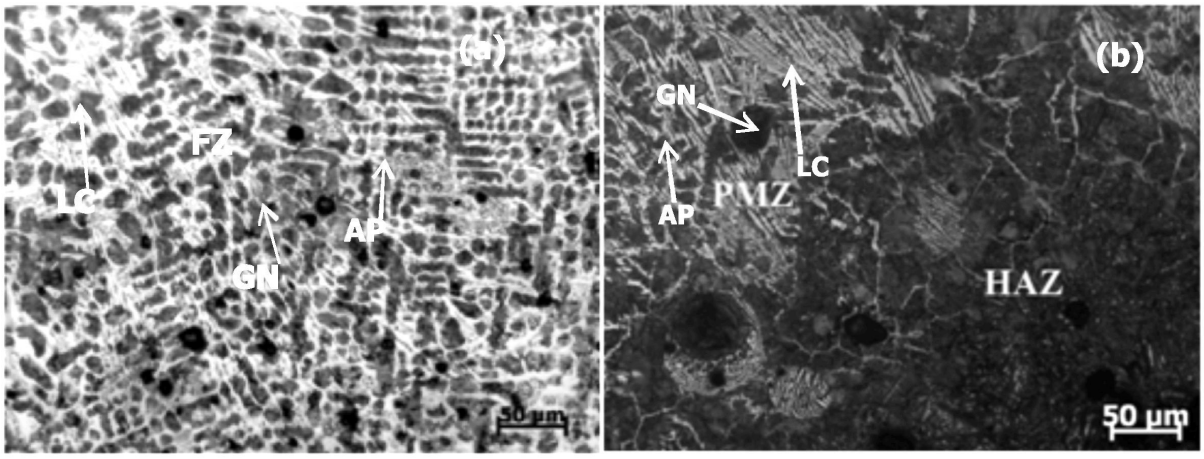


**Fig. 9** : Optical microstructure of (a) FZ,(b) PMZ and HAZ using Trial 3 electrode.

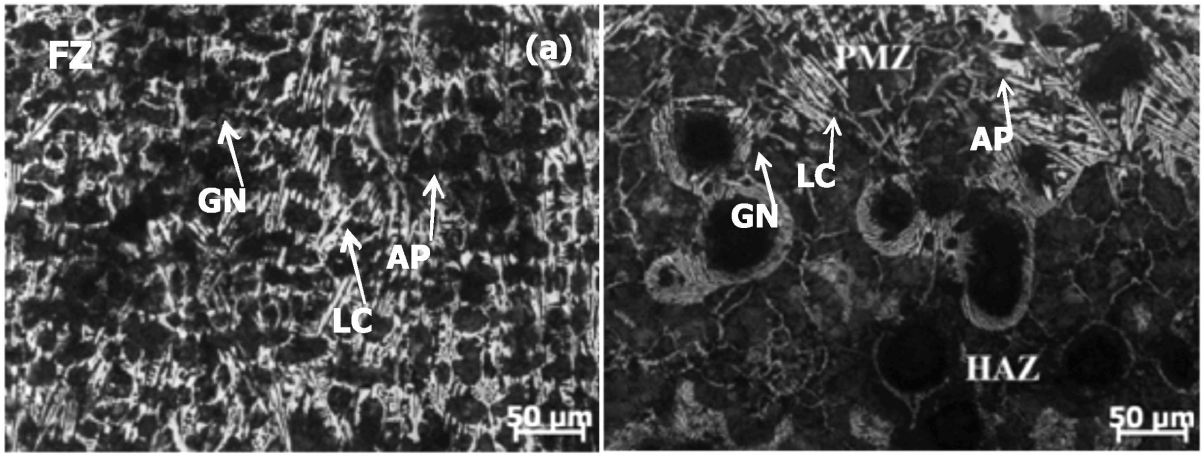


**Fig.10** : Optical microstructure of (a) FZ, (b) PMZ and HAZ using Trial 4 electrode.

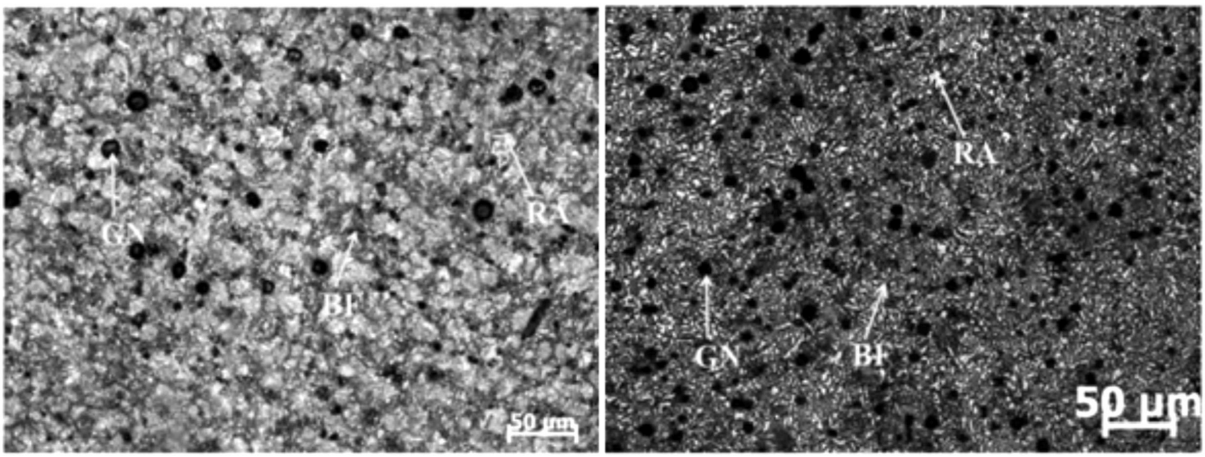


**Fig. 11** : Optical microstructure of weld deposited bead-on-plate using Trial 3 electrode austempered at (a) 300°C and (b) 350°C with 2hr holding time.

by three dimensional transfer of heat to the surrounding solid thereby enabling more rapid cooling rates to be experienced than from the overall two dimensional heat flow. However, the preheat at 300°C which is above the calculated martensite start (Ms) temperature of weld deposits, i.e., about 250°C, avoided martensite formation [38].

The portion of the HAZ was experienced temperature above the critical temperature show that austenite formed during the weld pass. The amount of C dissolve from graphite nodules in austenite depended on the peak temperature reached during the welding pass. The microstructures of HAZ exhibited pearlite and bainite with graphite nodules shown in the **Fig. 9 (b)** and **Fig. 10 (b)**.

### 3.5 Microstructure of the Weld Deposits after Austempering Heat Treatment

**Fig. 11 (a-b)** and **Fig. 12 (a-b)** show the optical micro-structures of the heat treated samples after austempering at 300°C and 350°C for 2 hrs. The austempered microstructure appears to be bainitic ferrite (needle-shaped) and retained austenite based matrix with graphite nodules (**Figs. 11 (a)** and **12 (a)**). Increasing the austempering temperature a change in the shape of the bainitic ferrite is observed (**Figs. 11 (b)** and **12 (b)**). SEM microstructures in **Figs. 13 (a-b)** and **14 (a-b)** clearly revealed the different phases in both lower and higher austempering temperature. At lower austempering temperatures (300°C), very fine needle-shaped bainitic ferrite characteristic of lower bainitic structure and retained austenite were detected (**Figs. 13 (a)** and **14 (a)**). On the other hand, at higher austempering temperatures (350°C), coarse and feathery bainitic ferrite characteristic of upper bainitic structure was observed (**Figs. 13 (b)** and **14 (b)**).

Total absence of carbide structure present in the weld deposits microstructure indicates that the austenitizing temperature 900°C is sufficient to cause the dissolution of high amount of carbide in weld deposits. During the austempering periods, the

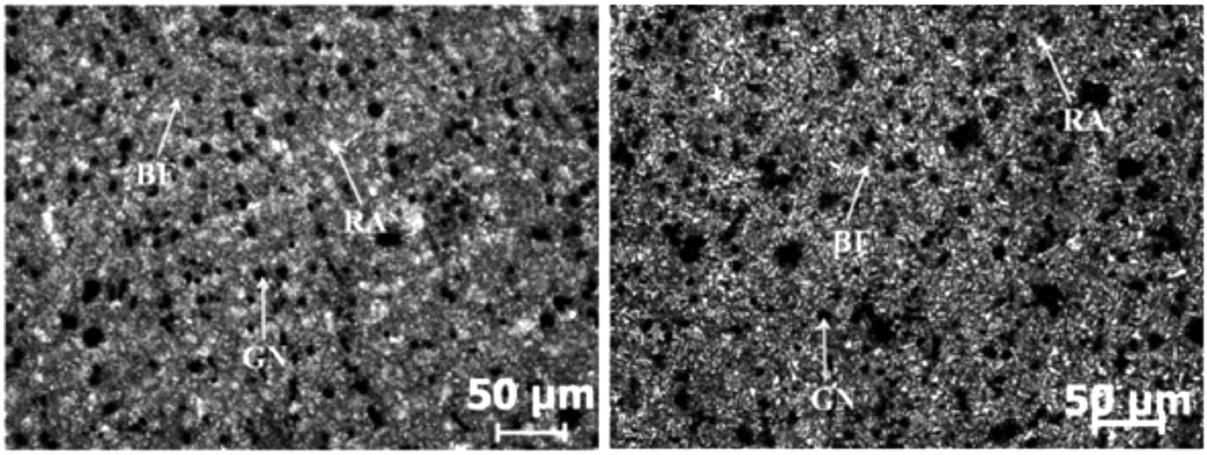


**Fig. 12 :** Optical microstructure of weld deposited bead-on-plate using Trial 4 electrode austempered at (a) 300°C and (b) 350°C with 2hr holding time.

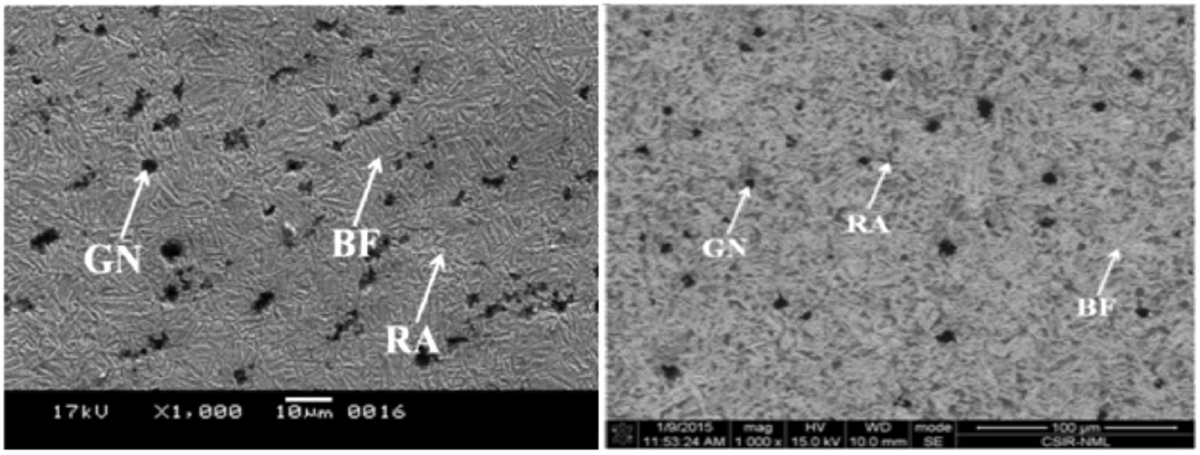


**Fig. 13 :** SEM microstructure of weld deposited bead-on-plate using Trial 3 electrode austempered at (a) 300°C and (b) 350°C with 2h holding time.

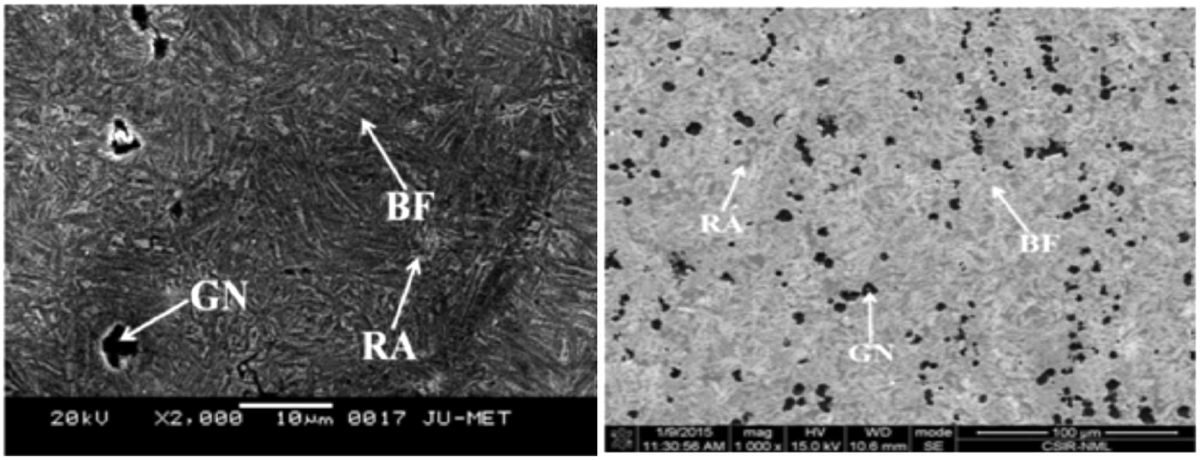


**Fig. 14 :** SEM microstructure of weld deposited bead-on-plate using Trial 4 electrode austempered at (a) 300°C and (b) 350°C with 2hr holding time.

nucleation of bainitic ferrite occurred at the interface of the residual austenite/graphite [39] and grew by the continuous nucleation of further plates into residual austenite. At the time of growing bainitic ferrite rejected carbon into the residual austenite and transformed to retained austenite which is stable at room temperature. Due to the growth of bainitic ferrite sheaves away from the graphite, these regions of supersaturated retained austenite exist in areas away from nodules.

The volume fraction of retained austenite ($X\gamma$) was determined by X-ray diffraction and peak intensity is shown in **Fig. 15 (a-b)**. The values of % retained austenite are given in **Table 6**. The retained austenite content ($X\gamma$) was observed to increase with increase in austempering temperature from 300°C to 350°C. This is because of the fact that during the austempering process, the ferrite forms out of austenite and since ferrite dissolves very little carbon (0.02%), for the ferrite needles to grow; the carbon from ferrite must diffuse out into the surrounding austenite [40] leading to increase in austenite stability. Thus with more time expended at particular temperature more retained austenite is expected.

### 3.6 Micro-hardness

The micro hardness values of different zones e.g. FZ, HAZ and BM of as-welded samples for both the electrodes (Trial 3 and Trial 4) are shown in **Fig. 16**. Due to presence of hard ledeburitic carbide present the FZ shows higher hardness values (~613Hv for Trial 3 and ~580Hv for Trial 4). However, relatively lower hardness of FZ in Trial 4 compare to Trial 3 is mainly due to lesser and discontinuous ledeburite carbide. Hardness values decreased in the HAZ, due to absence of ledeburitic carbide. However, HAZ with bainite and pearlite attributes higher hardness than basemetal which shows

**Table 6 :** Quantification of microstructural constituents and micro-hardness present in different heat treated weld deposits using Trial 3 and Trial 4 electrodes

| Using Electrode | Austempering conditions | | Microstructural Constituents | | Micro-hardness (Hv) |
|---|---|---|---|---|---|
| | °C | Time | Retained austenite (Vol.%) $X\gamma$ | Bainitic cerrite (Vol. %) | |
| Trial-3 | 300 | 2 | 40.01 | 59.99 | 338.9 |
| | 350 | 2 | 41.24 | 58.76 | 313.76 |
| Trial-4 | 300 | 2 | 39.44 | 60.56 | 330.08 |
| | 350 | 2 | 41.55 | 58.45 | 329.91 |

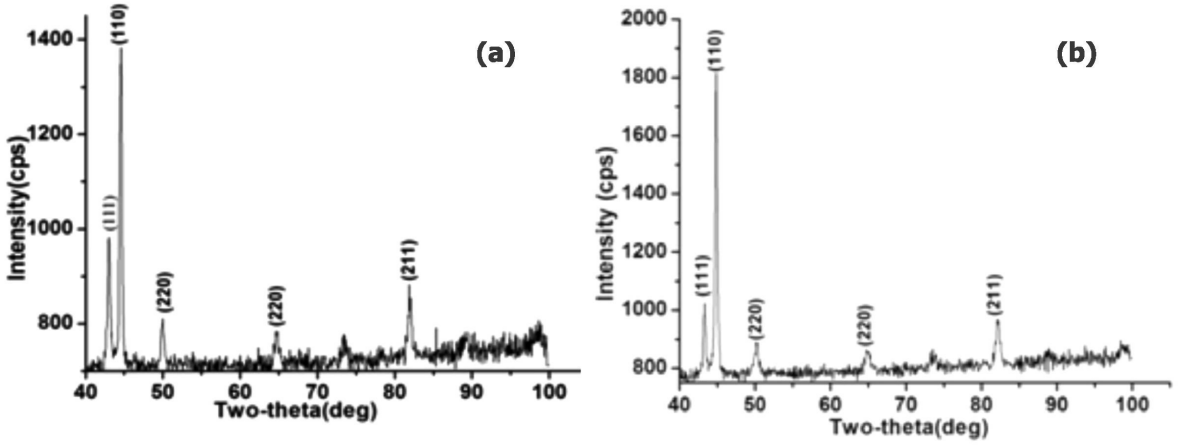


**Fig.15 :** XRD plot for calculating retained austenite at (a) Trial 3and (b)Trial 4 austempering at 350°C austempering for 2hr.

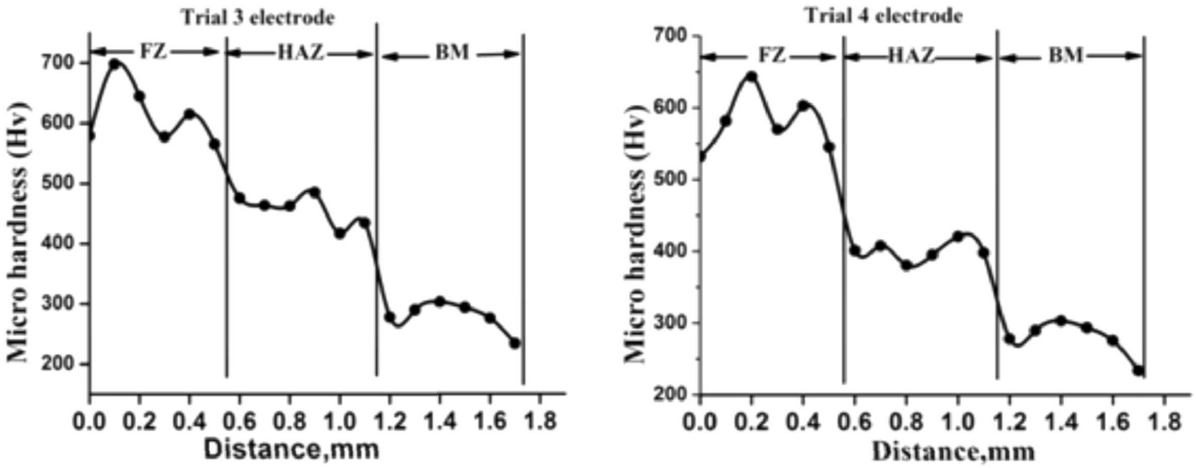


**Fig. 16 :** Micro hardness distribution of different zone of the structure using (a) Trial 3 and (b) Trial 4 electrode.

ferrite/ pearlite matrix. The average hardness values of heat treated weld deposits are given in **Table 6**. It is clearly observed from **Table 6** that with increasing austempering temperature the hardness decreases.

## 4.0 CONCLUSIONS

The results obtained in this study leads to the following conclusions:

- Among the six different coated electrodes developed, Trial 3 and Trial 4 electrodes showed compatible to ADI.
- Welding conditions differed for Trial 3 and Trial 4 electrodes. Trial 4 electrode required only preheat at 300ºC for 1 hr to produce crack free weld deposits; whereas both preheat and post weld heat treatment (PWHT) at 300ºC for 1 hr immediately after welding were required for Trial 4 electrode.
- Microstructures of different zones in as-welded DI varied considerably using Trial 3 and Trial 4 electrodes. More ledeburitic carbide and less alloyed pearlite were observed in FZ and PMZ using Trial 3 compared to Trial 4. However, microstructures of HAZ for both the electrodes showed bainite and pearlite
- Austempering heat treatment comprising of austenitized at 900°C for 2 hr and then austempered at two different temperatures e.g. 300°C and 350°C was performed to understand the austempering response of two weld depositsusing Trial 3 and Trial 4. Interestingly. Austempered microstructures for both the weld deposits show bainitic ferrite and retained austenite with graphite nodules. However, increasing austempering temperature from 300°C to 350°C, the lower bainitic ferrite transformed to upper bainitic ferrite and vol. % of retained austenite increased.
- Microhardness values changed significantly across the as-welded deposit. FZ showed maximum hardness valuedue to presence of ledeburitic carbide and the hardness of HAZ was maintained between FZ and BM.

## REFERENCES

1. C. Mon, M.H. Tierean, A review of tests of austempered ductile iron welding, Bulletin of the Transilvania University of Brasov. Vol, 8 (57) p.1-2015
2. S.K. Putatunda, A.V. Singara, R. Tackett, G. Lawes, Development of a high strength high toughness ausferritic steel, Materials Science and Engineering A, 513–514 (2009), pp. 329–339
3. L. Bartosiewicz, A.R. Krause, F.A. Alberts, I. Singh, S.K. Putatunda, Influence of microstructure of high cycle behaviour of austempered ductile iron, Mater. Character., 30 (1993), pp. 221-234.
4. S.K. Putatunda, Development of austempered ductile cast iron (ADI) with simultaneous high yield strength and fracture toughness by a novel two-step austempering process, Mater. Sci. Eng., A 315 (2001), pp. 70-80.
5. Y.J. Kim, H. Shin, P.J.D.H. Lim, Investigation into mechanical properties of austempered ductile cast iron (ADI) in accordance with austempering temperature, Mater Lett 62 (2008) pp.357–60.
6. Y.S. Lerner, G.R. Kingsbury, Wear resistance properties of austempered ductile iron, J Mater Eng Perform, 1998, 7, pp.48–52.

7. L. Magalhaes, R. Martins, J. Seabra, Low-loss austempered ductile iron gears : experimental evaluation comparing materials and lubricants, Tribol Int, 2012; 46, pp.97–105.
8. J. Lefevre, K.L. Hayrynen, Austempered materials for powertrain applications, J Mater Eng Perform, 2013, 22, pp.1914–1922.
9. J. Panasiewicz, C. Grupke, J. Huth, Chrysler's experience with austempered ductile iron, in: Proceedings of the World Conference on Austempered Ductile Iron, Bloomingdale, IL, March 1991, pp. 176-194.
10. K. Okazaki, H. Asai, M. Tokuyoshi, H. Kusonoki, H. Sakahara, Proceeding of the World Conference on Austempered Ductile Iron, Bloomingdale, IL, March 1991, pp. 288-299.
11. B.V. Kovacs. Austempered ductile iron, facts and fiction, Mod. Cast, 36 (1990), pp. 38–41.
12. E.E. Huke, H. Udin, Welding metallurgy of nodular cast iron. Weld J, 1953, 32, pp.378s–385s.
13. E.F. Nippes, The heat affected zone of arc welded ductile iron, Weld J, 1960, 39, pp.465–472.
14. G.R. Pease, The welding of ductile iron, Weld J, 1960, 39, pp.1–9.
15. S.D. Kiser, Production welding of cast iron, AFS Trans, 1977, 85, pp.37–42.
16. G.R. Pease, The welding of ductile iron, Weld J, 1960, 39, pp.1–9.
17. H. Cetain, Fracture behaviour of overmatched ductile iron, Int. J. Mater, Res, 2007, 198, pp.128-136.
18. S.D. Kiser, B. Irving, Unravelling the mysteries of welding cast iron. Weld J, 1960, 72, pp. 39-44.
19. N. Fujii, H. Honda, A. Fukase, K. Yasuda, Comparison of strength characteristic of nodular graphite cast iron welded joints by various welding process, Quart J Jpn Weld Soe, 2007, 25, pp.261-277.
20. R.C. Voight, C.R. Loper Jr., A study of heat affected zone structure in ductile cast iron, Weld Soc., 2007, 25, pp.261-267.
21. R.A. Martinez, J.K. Sikora, Perlitic nodular cast iron: can it be welded, Weld J, 1995, pp. 65-70.
22. E.M. El-Banna, Effect of preheat on welding of ductile cast iron, Mater Lett, 1999, 41, pp. 20-26.
23. D.J. Kotecki. N.R. Braton, N.R. Loper, Preheat effect on gas metal arc welding ductile cast iron, Weld J, 1969, 48, pp. 161s-166s.
24. E.M. El-Banna, M.M. Nageda, Abo El-Saadat, Study of restoration by welding of pearlitic ductile cast iron. Materials Letters, 2000, vol. 42, pp. 311-320.
25. K. Ishizaki., J.G. Moram., S.L. Marifler, A. Davila, Simulation study on ductile cast iron welding by austenitic filler metal. Trans. of Japan Welding Society, 15 (2), 1984, pp.3-9.
26. D.R. Askeland, N. Birer, Secondary graphite formation in tempered nodular cast iron weldment, Weld J, 52 (1979), pp.337s-341s.
27. D. Rach, Filler metals for cast iron welding, Tech. Report Messer Grieshaiem, Germany, pp.1-11.
28. R.A. Bishel, H.R. Conaway, Flux-coard arc welding for high-quality joints in ductile iron, AFS Trans. 84 (1976), pp. 487-492.
29. E.E. Huke, H. Udin, Welding metallurgy of nodular cast iron, Weld.J, 32 (1953), pp. 378s-385s.
30. R.A. Martines, J.A. Ashikera, Pearlitic nodular cast iron: can it be welded?, Weld. J, 74 (1995), pp. 65s-70s.
31. M. Pascual, C. Ferrer, Y.E. Rayon, Weldability of spherodial graphite cast iron using Ni/Ni-Fe electrodes, Revista de Metalurgia, 45(5), (2009), pp.334-338.
32. D.Q. Sun, X.Y. Gu, W.H. Lui, Z.Z. Xuan, Welding consumable research for austempered ductile iron (ADI), Material Science and Engineering A, 402 (2005), pp. 9-15.
33. C.E. Jackson. Flux and Slag in Welding. Weld Res. Bull. 1973, No.190, Welding Research Council, New York, N.Y.
34. Linnert, G.E. 1965. Welding Metallurgy. American Welding Society, Miami, Fla., Vol.1, Ch.8, pp.367-396.
35. Kou, S., Welding Metallurgy, 2nd edition, New Jersy: John Wiley and Sons, 2003.
36. K.B. Rundman, R.C. Klug, AFS Trans. 90 (1982) pp. 499–508.
37. G.E. Linnert, Welding-Metallurgy, 3rd Ed, AWS, 1965, Vol.1.
38. R.C. Voigt, C.R. Loper Jr, A study of heat affected zone structures in ductile cast iron, AWS,1982, pp.82-88.
39. J.S. James, Microstructural Modelling of ADI Camshafts, Ph.D. Thesis, Loughborough University, UK, 1999.
40. Y. Jianghuai, S.K. Putatunda, Influence of a novel two-step austempering process on the strain-hardening behaviour of austempered ductile cast iron (ADI), Materials Science and Engineering A, 382, 2004, pp.265–279.